JACS
JOURNAL OF THE AMERICAN CHEMICAL SOCIETY
Article
pubs.acs.org/JACS

Molybdenum-Carbide-Modified Nitrogen-Doped Carbon Vesicle Encapsulating Nickel Nanoparticles: A Highly Efficient, Low-Cost Catalyst for Hydrogen Evolution Reaction

Shiping Wang, Jing Wang, Minglei Zhu, Xiaobing Bao, Bingyang Xiao, Diefeng Su, Haoran Li, and Yong Wang*

Advanced Materials and Catalysis Group, ZJU-NHU United R&D Center, Center for Chemistry of High-Performance and Novel Matrials, Key Lab of Applied Chemistry of Zhejiang Province, Department of Chemistry, Zhejiang University, Hangzhou 310028, P. R. China

Supporting Information

ABSTRACT: Despite being promising substitutes for noble metal catalysts used in hydrogen evolution reaction (HER), the nonprecious metal catalysts (NPMCs) based on inexpensive and earth-abundant 3d transition metals (TMs) are still practically unfeasible due mainly to unsatisfactory activity and durability. Herein, a highly active and stable catalyst for HER has been developed on the basis of molybdenum-carbide-modified N-doped carbon vesicle encapsulating Ni nanoparticles (Mo_xC-Ni@NCV). This Mo_xC-Ni@NCV material was synthesized simply by the solid-state thermolysis of melamine-related composites of oxalate and molybdate with uniform Ni ions doping (Ni@MOM-com). Notably, the prepared Mo_xC-Ni@NCV was almost the most efficient NPMCs for HER in acidic electrolyte to date. Besides good long-term stability, Mo_xC-Ni@NCV exhibited a quiet low overpotential that was comparable to Pt/C. Thus, this work opens a new avenue toward the development of highly efficient, inexpensive HER catalysts.

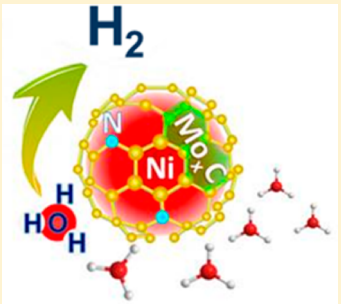

INTRODUCTION

The production of hydrogen has drawn extensive attention because of its relevance to clean and renewable energy technologies.[1,2] The electrocatalytic hydrogen evolution from water splitting is one of the acknowledged powerful routes to produce hydrogen for the abundant hydrogen source and high energy conversion efficiency.[3] Because of the extremely high activity for hydrogen evolution reaction (HER), noble metals (e.g., Pt, Pd) are currently adopted as the main HER catalysts.[4−6] However, this kind of catalyst is costly and limited in resources, hindering the global scalability of the HER technology. Over the past few decades, much effort has been made to develop inexpensive and earth-abundant 3d transition metals (TMs), such as Fe, Co, and Ni, as promising nonprecious metal catalysts (NPMCs) for HER, and the improvement of activity and durability for HER is the main target of these studies.[7−10] It is considered that the electrocatalytic HER is more exquisite in acidic electrolyte than alkaline electrolyte, while the general 3d TMs,[11−13] alloys,[14−16] and oxide[17] catalysts are not attractive in acidic electrolytes due to their poor stability. Although the TM sulfides,[18−22] nitrides,[23−25] borides,[26] and phosphides[27−29] have been demonstrated as possible alternative catalysts for HER in acidic electrolyte, the catalytic HER activity of these catalysts is disappointing in comparison to noble metal catalysts.

While TM-based catalysts are supported on porous carbon materials, excellent performances can be presented for a variety of electrocatalytic systems (e.g., HER), owing to the relatively high porosity, great electronic conduction, as well as strong corrosion resistance under both acidic and alkaline conditions.[30−33] Generally, TM-based active sites supported on the surface of porous carbons are easily exposed to the electrolytes, causing possible irreversible degradation. Recently, TM-incorporated carbon composites have been proposed as improved catalysts for HER.[34−38] For instance, nitrogen-doped carbon nanotubes encapsulating Fe, Co, and FeCo alloy (TMs@NCNTs), which could efficiently catalyze the HER with high activity and long-term durability in acidic electrolytes, were synthesized by a chemical vapor deposition method.[37,38] On the basis of the theoretical calculations and experimental results, the synergistic effect of the nitrogen dopants and TMs nanoparticles can enrich the electron density on the carbon surface, promoting the hydrogen adsorption and evolution.[36,38] This is mainly attributed to the lone-pair electrons of the graphitic N, pyridinic N, and pyrrolic N in the TMs@NCNTs materials. Moreover, active TM nanoparticles encapsulated in the ultrathin graphene layers were reported to enhance the HER performance in acidic electrolyte due to their improved electron penetration.[34,36] Nevertheless, researchers are still very eager for new efficient and economic techniques to improve the HER activity of TM-based catalysts.

Because of their unique d-band electronic structures and similar catalytic properties to Pt group metals, group VI

Received: August 12, 2015
Published: December 1, 2015

DOI: 10.1021/jacs.5b07924
J. Am. Chem. Soc. 2015, 137, 15753−15759

transition-metal carbides are favorable for enhancing the activity and stability of electrocatalysts.[39−43] Among these group VI transition-metal carbides, molybdenum carbides have been recently investigated intensively, especially Mo_2C.[44−47] For example, a nanoporous Mo_2C nanowire was developed as a highly active and stable electrocatalyst for HER in acidic electrolytes.[46] Anchored into the porous carbon supports, the Mo_2C nanoparticles exhibited enhanced catalytic HER activity and stability for the electronic modification and relatively moderate strength for the Mo−H bond.[42] Apart from being electrocatalysts, Mo_2C was also employed as efficient supports for diverse catalysts to enhance their catalytic activity and stability.[44,45] Compared with Mo_2C, γ-MoC is more stable and formed at higher temperature (>900 °C).[42,43] In particular, it has been confirmed that γ-MoC is more effective in promoting the activity and stability of Pt-based catalyst in the oxygen reduction reaction (ORR) due to different synergistic effects and binding energy.[45] To the best of our knowledge, there are few studes related to the exploration of γ-MoC used in HER.

Herein, a novel Ni-encapsulated nitrogen-doped carbon vesicle material modified by molybdenum carbides (γ-MoC and β-Mo_2C) (Mo_xC-Ni@NCV), which was very active and stable for HER in acidic electrolyte, was synthesized by a solid-state thermolysis method at relatively low temperature. In this method, water-insoluble melamine-related composite of oxalate and molybdate with uniform Ni ions doping (Ni@MOM-com) was pre-prepared in aqueous solution and used as the precursor of solid-state thermolysis. The effects of Ni and Mo sources on the structure and composition of the products were investigated in detail. In addition, to evaluate the catalytic HER performance of the prepared Mo_xC-Ni@NCV material, the linear sweep voltammetry curves (LSV) and time-dependence catalytic current graphs were measured in both acidic (0.5 M H_2SO_4) and alkaline (1 M KOH) electrolytes. Furthermore, the influences of textural properties and compositions of the Mo_xC-Ni@NCV material on its catalytic HER activity were studied in order to synthetically understand the catalytic performance.

EXPERIMENTAL SECTION

Materials. Melamine was purchased from Aladdin Chemistry Co., Ltd. Nickel chloride hexahydrate ($NiCl_2·6H_2O$), ammonium molybdate tetrahydrate ($(NH_4)_6Mo_7O_{24}·4H_2O$), and oxalic acid dihydrate ($C_2H_2O_4·2H_2O$) were purchased from Sinopharm Chemical Reagent Co., Ltd. The above chemicals were analytical grade and used as received. 5 wt % Nafion 117 solution was purchased from Sigma-Aldrich Chemistry Co., Ltd. Deionized water was used as the solvent.

Synthesis of Materials. The preparation processes for different samples were basically the same. The addition amount of $C_2H_2O_4·2H_2O$ and melamine remained unchanged with a molar ratio of 2:1. Typically, the molybdenum-carbide-modified nitrogen-doped carbon vesicle encapsulating Ni nanoparticles (Mo_xC-Ni@NCV) was synthesized as follows. First, 2.52 g (0.02 mol) of $C_2H_2O_4·2H_2O$ and 0.27 g (0.0015 mol) $(NH_4)_6Mo_7O_{24}·4H_2O$ were dissolved in 40 mL of deionized water. After that, 1.26 g (0.01 mol) melamine was added, and the mixture was refluxed at 70 °C for 6 h under stirring condition. Then, 10 mL of 1 M $NiCl_2·6H_2O$ (2.4 g, 0.01 mol) was added into the mixture solution, stirring at room temperature for 12 h. After filtration, the insoluble precipitate was washed with deionized water and dried at 70 °C. By this way, the melamine-related composite of oxalate and molybdate Ni@MOM-com was formed, which was used as the precursor. Subsequently, the precursor was calcined at 900 °C for 2 h with a heating rate of 10 °C min^{-1} in N_2 flow. In order to investigate the formation mechanism and the effects of different addition of Ni, Mo source, other samples were prepared according to Table S1 (Supporting Information). The obtained products were denoted as sample xMoyNi@T, where x and y, respectively, represented the addition amount (g) of Mo source ($(NH_4)_6Mo_7O_{24}·4H_2O$) and Ni source ($NiCl_2·6H_2O$), and the T referred to the calcination temperature.

Characterizations. Scanning electron microscopy (SEM) images were measured on a Hitachi SU-70 electron microscope at an acceleration voltage of 25.0 kV. Transmission electron microscopy (TEM) images were presented on a Hitachi HT-7700 microscope at 80.0 kV. Nitrogen sorption isotherms were obtained on an ASAP 2020 V 3.00 H surface area and porosity analyzer. On the basis of the isotherms, specific surface area was calculated via a multipoint method from the adsorption data, and the pore size distribution was analyzed by the DFT method from the desorption data. Element contents were provided on a Vario EI elemental analyzer. Inductively coupled plasma atomic emission spectrometry (ICP-AES) was employed to determine the Ni, Mo contents in the products, which were dissolved in 70 wt % nitric acid. The distributions of various elements in the products were exhibited by X-ray photoelectron spectroscopy (XPS) on an ESCALAB 250Xi spherical analyzer. The XRD data were collected on a D/tex-Ultima TV wide-angle X-ray diffractometer equipped with Cu Kα radiation. The Raman spectra were recorded on a Raman spectrometer (JY, HR 800) using 514 nm laser.

Electrochemical Measurements. The catalytic performance of the prepared samples for hydrogen evaluation reaction was measured with a three-electrode cell by linear sweep voltammetry (LSV) method on a computer controlled CHI electrochemical workstation: the counter electrode was a platinum sheet with a surface area of 1 cm^2, the reference electrode was a saturated calomel electrode (SCE), and the working electrode was a glassy carbon (5 mm in diameter) supporting the measured materials. The measured materials (6 mg) were predispersed in the mixture solution of 100 μL 5 wt % nafion solution and 1000 μL dehydrated ethanol by ultrasonication for 30 min. A 40 μL portion of the as-prepared ink was dropped on the surface of the glassy carbon, yielding a working electrode with a loading of 1.1 mg cm^{-2} after air-drying. For comparison, the commercial 20 wt % Pt/C was supported on the glassy carbon with the same loading. The LSV curves of different samples were recorded without solution agitation at a scan rate of 10 mV s^{-1} in 0.5 M H_2SO_4 or 1 M KOH solution that was purged with N_2 flow. The electrochemical impedance spectroscopy (EIS) was recorded on a Gamry reference 600 instrument. All the measurements were performed at room temperature. The potentials in the final graphs were converted to the potentials versus the reversible hydrogen electrode (vs RHE) according to the following calculation: E (vs RHE) = E (vs SCE) + E°_{SCE} + 0.0592 pH. The overpotential values were described by the Tafel equation $\eta = a + b \log j + jR_s$, where η (V) denotes the applied overpotential, j (A cm^{-2}) is related to the current density, b (V dec^{-1}) represents the Tafel slope, and R_s (Ω cm^{-2}) is the total area-specific uncompensated resistance of the system.

RESULTS AND DISCUSSION

In this study, the molybdenum-carbide-modified N-doped carbon vesicle encapsulating Ni nanoparticles (Mo_xC-Ni@NCV) was synthesized by the solid-state thermolysis of rod-like melamine-related composite of oxalate and molybdate with uniformly doped Ni ions (Ni@MOM-com) (Figure S1). Representatively, sample 0.27Mo2.4Ni@900 was produced from a Ni@MOM-com precursor with 0.27 g Mo source and 2.4 g Ni source additions. Scanning electron microscopy (SEM) images revealed that the products were aggregated from a rod-like structure that was assembled from nanoparticles about 31 nm in diameter (Figure 1 a,b). Transmission electron microscopy (TEM) image showed that these nanoparticles were closely interconnected hollow vesicles of 3−35 nm in diameter along with some solid nanoparticles (Figure 1c). The N_2 sorption isotherm of sample 0.27Mo2.4Ni@900 presented a hysteresis loop, suggesting that the products held a mesoporous

DOI: 10.1021/jacs.5b07924
J. Am. Chem. Soc. 2015, 137, 15753−15759

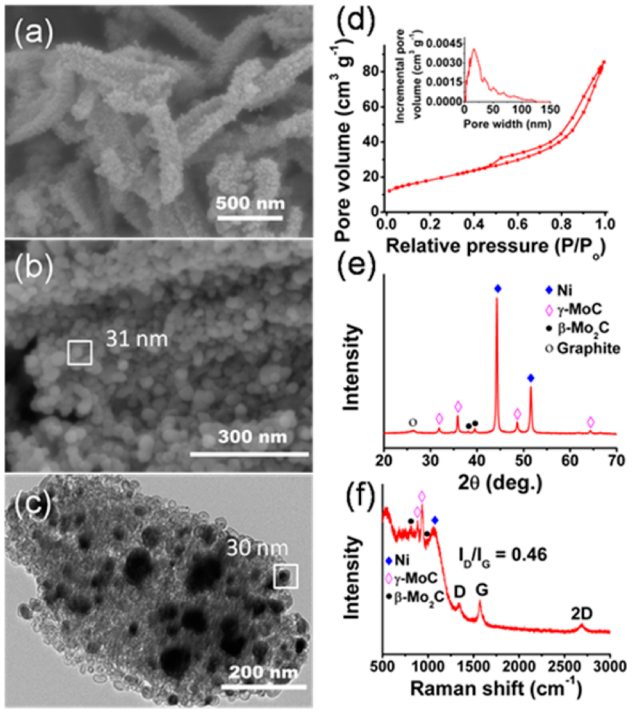

Figure 1. Characterizations of 0.27Mo2.4Ni@900: (a and b) SEM images, (c) TEM image, (d) N_2 sorption isotherms and the corresponding pore width distribution (inset), (e) XRD pattern, (f) Raman spectrum.

structure (Figure 1d). Besides, the pore width distribution of sample 0.27Mo2.4Ni@900 demonstrated that mesopores in a wide range of 2−50 nm as well as macropores were formed in the products (the inset of Figure 1d). In addition, the specific surface area and micropore volume of the sample 0.27Mo2.4Ni@900 were, respectively, 65 m^2 g^{-1} and 0.006 cm^3 g^{-1}, which confirmed that few micropores existed in the material (Table S2). These provided sufficient evidence that sample 0.27Mo2.4Ni@900 had a hierarchically mesoporous structure, which was favorable for mass transport and adsorption.

The powder X-ray diffraction (XRD) patterns confirmed that sample 0.27Mo2.4Ni@900 was composed of graphite, metallic Ni, γ-MoC and β-Mo_2C (Figure 1e). On the basis of the linear intensities of the main peaks of γ-MoC (100) and ß-Mo_2C (101), the weight ratio of γ-MoC to β-Mo_2C was estimated to be about 3:1.[48] The graphite nature was investigated by Raman spectrum (Figure 1f), which revealed a high graphitization degree with an I_D/I_G value of 0.46, being advantageous for electron transfer. The X-ray photoelectron spectroscopy (XPS) indicated that C, N, O, Ni and Mo elements existed in the sample 0.27Mo2.4Ni@900 (Figure S2). To further identify the states of C, N, Ni and Mo species, their high-resolution XPS spectra were analyzed in detail. As shown in Figure S3, four C species appeared in the C 1s XPS spectrum. Particularly, the peak related to molybdenum carbides occurred at 282.7 eV. The N 1s XPS spectrum showed two N peaks at 398.2 and 401.1 eV, which respectively originated from the pyridinic N (81%) and graphitic N (19%) (Figure S3b). Due to their lone-pair electrons, these species of N can synergistically tune the electron density on the surface of graphene layers with the encapsulated Ni nanoparticles.[36,38] For the Ni 2p XPS spectrum (Figure S3c), the peaks at 852.7 and 870.1 eV belonged to the elemental Ni whereas the signals situated at 854.8 and 872.8 eV were possibly caused by the Ni−C bond on the surface of Ni nanoparticles. In addition, Figure S3d revealed that there were four oxidation states for Mo (Mo^0, Mo^{3+}, Mo^{4+} and Mo^{6+}) in the Mo_xC-Ni@NCV material. The dominant Mo^0 peaks and small Mo^{3+} peaks can be attributed to the Mo−Mo and Mo−C bonds in molybdenum carbides.[49] As explained by previous studies, the high oxidation states (Mo^{4+} and Mo^{6+}) originated from the contamination of the molybdenum carbide's surface.[50]

As determined by the elemental analysis, the C content of sample 0.27Mo2.4Ni@900 was about 23.54 wt % (Table S3). Also, the Ni and Mo contents were, respectively, 58.80 and 14.95 wt % as measured by the inductively coupled plasma atomic emission spectrometry (ICP-AES) (Table S3). Besides, the X-ray photoelectron spectroscopy (XPS) exhibited that C, Ni, and Mo contents of sample 0.27Mo2.4Ni@900 were 68.93, 8.80, and 7.56 wt %, respectively (Table S4). These results indicated that the majority of metallic Ni and some molybdenum carbides were embedded in carbon, which was also proven by the HR-TEM images (Figure 2 and Figure S4).

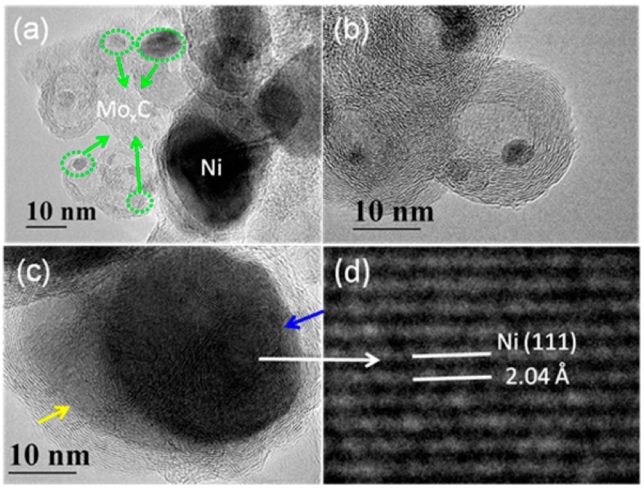

Figure 2. (a, b) Low-resolution HR-TEM images of sample 0.27Mo2.4Ni@900. (c) Low-resolution HR-TEM image of the Ni nanocrystals in sample 0.27Mo2.4Ni@900. (d) Higher-resolution HR-TEM image of the Ni nanocrystals in sample 0.27Mo2.4Ni@900.

The low-resolution HR-TEM images indicated that some solid nanoparticles were encapsulated in the graphene layers that were similar to the shells of the hollow vesicles (Figure 2a,b). The nanoparticles labeled by green circles in Figure 2a were molybdenum carbides (γ-MoC and β-Mo_2C) as confirmed by Figure S4a, and the majority of these particles were less than 10 nm. In addition, the HE-TEM image (Figure S4) and EDX measurements (Figure S5, labeled by green circle) also indicated that a few of molybdenum carbide nanoparticles were about 10 nm. Also, Figure S4 revealed that molybdenum carbides were also modified on the surface of Ni-encapsulated graphene layers. The white arrow in Figure 2c exhibited the nanocrystal with an interplanar spacing of 2.04 Å (Figure 2d), with an assignment to the (111) crystal plane of metallic Ni. These Ni nanocrystals held a particle size about 30 nm and were encapsulated in graphene layers as labeled by the yellow arrows in Figure 2c. Besides that, the blue arrow in Figure 2c showed clear graphene vesicles around the carbon encapsulat-

DOI: 10.1021/jacs.5b07924
J. Am. Chem. Soc. 2015, 137, 15753−15759

ing Ni nanoparticle, which was in accord with the phenomenon observed in the TEM image (Figure 1c).

Moreover, the high-angle annular dark-field scanning transmission electron microscopy (HAADF-STEM) image and corresponding EDX mappings were measured to investigate the distributions of the existing elements in sample 0.27Mo2.4Ni@900. As shown in Figure 3, relatively uniform Ni nanoparticles

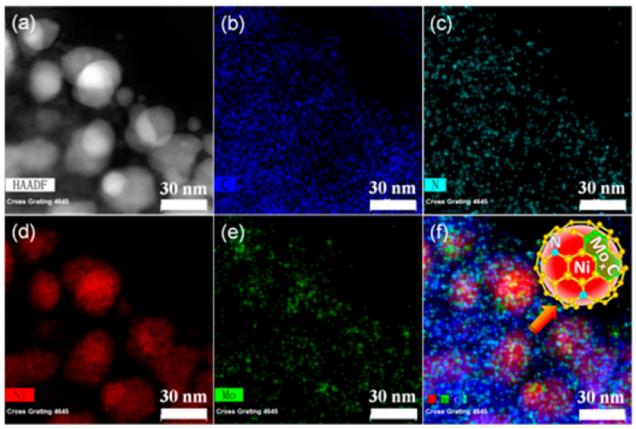

Figure 3. (a) HAADF-STEM image of sample 0.27Mo2.4Ni@900. (b–f) The corresponding EDX maps for C (b), N (c), Ni (d), Mo (e), and their combined image (f). The inset drawing is the schematic illustration of the Mo_xC-Ni@NCV structure.

were formed in the Mo_xC-Ni@NCV, and the C, N atoms were distributed homogeneously over this material. Of particular interest here is that the Mo atoms tended to distribute considerably over these Ni nanoparticles. Thus, it was implied that the molybdenum carbides were mainly modified over the Ni nanoparticles (the inset of Figure 3f).

Further studies indicated that the Ni source played a crucial role in the synthesis of hierarchically mesoporous Mo_xC-Ni@NCV material. With exclusive addition of the Mo source, sample 0.27Mo0Ni@900 was rod-like material modified with some nanoparticles about 6 nm in diameter (Figure S6a,b). This material was almost nonporous with a low surface area of 18 $m^2\ g^{-1}$ (Table S2 and Figure S6e,f). Besides, there was no γ-MoC, but β-Mo_2C existed in this material that had a relatively low degree of graphitization (I_D/I_G = 1.02) (Figure S7a,b). On the other hand, with exclusively adding the Ni source, sample 0Mo2.4Ni@900 exhibited the morphology and hierarchically mesoporous structure similar to sample 0.27Mo2.4@900 (Figure 1 and Figure S6c,d), and the I_D/I_G value (0.56) of sample 0Mo2.4Ni@900 was comparable to the value (0.46) of sample 0.27Mo2.4Ni@900 (Figure S7b). These phenomena confirmed that the addition of Ni source promoted the formation of highly graphitized mesoporous carbon for sample 0.27Mo2.4Ni@900. Generally, Co, Fe, or Ni species can catalyze the decomposition and graphitization of precursors to form diverse graphitized-carbon/metal composites (CMCs), and the structure of the CMCs is influenced by the precursor structure.[51−53] Accordingly, the Ni-encapsulated carbon vesicles were inferred to be synthesized on account of the poor supply of carbon in the Ni@MOM-com precursor. Besides, it was reported that some metal species such as $FeCl_2$ and NiI_2 can stabilize the γ-MoC phase upon reduction during the calcination process, so that the formation of γ-MoC in sample 0.27Mo2.4Ni@900 was possibly controlled by the Ni source added in the Ni@MOM-com precursor.[43]

The electrocatalytic HER performance of the prepared Mo_xC-Ni@NCV materials was investigated on a glassy carbon electrode in N_2-purged 0.5 M H_2SO_4solution. As control experiments, the catalytic HER activity of samples 0Mo2.4Ni@900 and 0.27Mo0Ni@900 were also studied under the same conditions. All the tested samples were deposited on a glassy carbon electrode with a similar loading of 1.1 mg cm^{-2}. It was demonstrated that both 0Mo2.4Ni@900 and 0.27Mo0Ni@900 showed very low current density (<7.5 mA cm^{-2}) even at a high overpotential of 300 mV, indicating a rather poorly catalytic activity for HER (Figure 4a). Significantly, with an

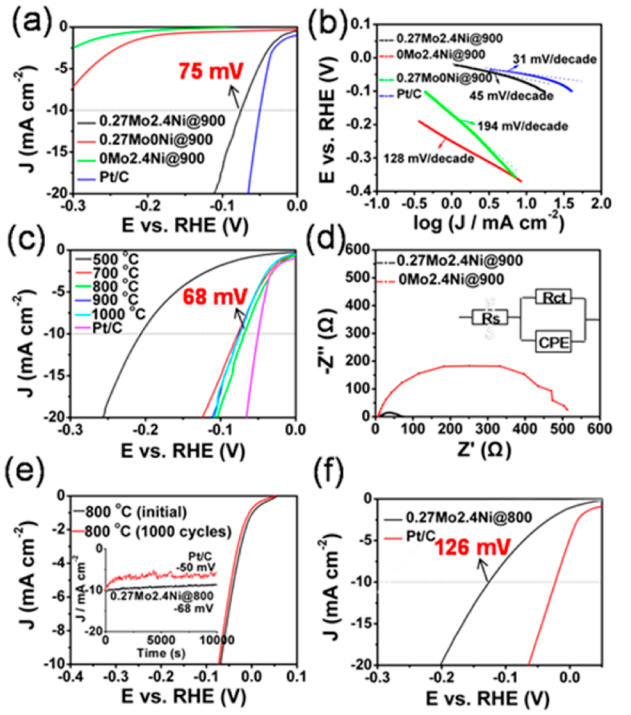

Figure 4. (a) Polarization curves measured in 0.5 M H_2SO_4 for Pt/C and samples prepared with the addition of different metal source. (b) Tafel plots for the corresponding samples in 0.5 M H_2SO_4. (c) Polarization curves in 0.5 M H_2SO_4 for samples prepared by calcination at different temperatures. (d) Nyquist plots measured at a voltage −75 mV (vs RHE) over the frequency range 100 kHz to 0.01 Hz in 0.5 M H_2SO_4. (e) Durability measurements in 0.5 M H_2SO_4: Polarization curves of sample 0.27Mo2.4Ni@800 recorded before the first and after 1000 CV sweeps between −142 and 108 mV (vs RHE) with a sweeping rate of 10 mV s^{-1}; inset is the time dependence of catalytic currents during electrolysis over 10 000 s for sample 0.27Mo2.4Ni@800 and commercial Pt/C. (f) Polarization curves for sample 0.27Mo2.4Ni@800 and Pt/C in 1 M KOH solution.

activation process caused by the removal of surface metal oxides (Figure S8−10), sample 0.27Mo2.4Ni@900 revealed highly catalytic HER activity in acidic electrolyte, implying a synergistic effect between γ-MoC and Ni. The HER catalyzed by sample 0.27Mo2.4Ni@900 reached stable state with an overpotential of 75 mV at a current density of 10 mA cm^{-2}, only 25 mV more than the value (50 mV) of the commercial 20 wt % Pt/C (Figure 4a). Notably, this overpotential was lower than the values of the currently most promising nonprecious metal catalysts (NPMCs) for HER in acidic electrolyte, including SCEIN/SWNT (77 mV),[34] Ni_2P (~120 mV),[28] CoNi@NC (142 mV),[36] Mo_2C/CNT (~150 mV),[42] and MoS_2/RGO (150 mV) (Table S5).[33] To the best of our

DOI: 10.1021/jacs.5b07924
J. Am. Chem. Soc. 2015, 137, 15753−15759

knowledge, the as-prepared Mo_xC-Ni@NCV materials displayed the most active NPMCs for HER in acidic electrolyte.

Furthermore, the mechanism of HER over the Mo_xC-Ni@NCV catalysts was studied by the Tafel plots measured in 0.5 M H_2SO4 solution. Typically, three elementary reactions were involved in the HER in acidic electrolyte. First, a proton associates an electron and attaches on the catalyst (*), namely, a Volmer reaction (eq 1). After that, the adsorbed H tends to form H_2 via the Heyrovsky or Tafel route, and sequentially desorbs. The Heyrovsky route is referred to the reaction of the adsorbed H with a hydrated proton from the electrolyte and receiving an electron from the catalyst surface (eq 2), while the Tafel route is related to the direct combination

$$H_3O^+ + e^- + * \rightarrow H^* + H_2O \quad (1)$$

$$H_3O^+ + e^- + H^* \rightarrow H_2 + H_2O \quad (2)$$

$$H^* + H^* \rightarrow H_2 \quad (3)$$

of two adsorbed H atoms (eq 3). Commonly, the HER mechanism can be determined by the Tafel slope of different catalysts. As shown in Figure 4 b, the Tafel slope and exchange current density of Pt/C were, respectively, 31 mV/decade and 3.16×10^{-3} A cm^{-2}, which was consistent with the Tafel mechanism that commonly occurred over Pt/C catalyst. Under the same conditions, sample 0.27Mo2.4Ni@900 exhibited a Tafel slope of 45 mV/decade and an exchange current density of 0.95×10^{-3} A cm^{-2}, indicating a Volmer–Heyrovsky mechanism. This Tafel slope was comparable to the values presented by the highly efficient HER NPMCs reported so far, for example, SCEIN/SWNT (40 mV/decade),[34] Ni_2P (~46 mV/decade),[28] Mo_2C/CNT (~55 mV/decade),[42] and MoS_2/RGO (~41 mV/decade).[33] In comparison, the Tafel slopes of samples 0Mo2.4Ni@900 (128 mV/decade) and 0.27Mo0Ni@900 (194 mV/decade) were much larger than that of sample 0.27Mo2.4Ni@900. In addition, the exchange current densities of sample 0Mo2.4Ni@900 and 0.27Mo0Ni@900 were, respectively, 0.24×10^{-3} and 0.35×10^{-3} A cm^{-2}, less than the value of 0.27Mo2.4Ni@900.

According to the above studies, the influences of the textural properties and compositions of the Mo_xC-Ni@NCV materials on the highly catalytic activity for HER were comprehensively analyzed. It was confirmed that sample 0Mo2.4Ni@900 had similar graphitization degree and textural properties (e. g., morphology, specific surface area and porous structure) to those for sample 0.27Mo2.4Ni@900, but their HER activities differed greatly. This first excluded the influences of graphitization degree and textural properties on the high HER activity of sample 0.27Mo2.4Ni@900. As reported, the nitrogen dopants in the CMCs have an important effect on the HER activity.[36,37] Especially, for these metal-nanoparticle-encapsulated carbon materials, the N dopants have been proven to synergistically increase the electron density on the graphene surface, which led to the improved HER activity. As shown in Tables S3 and S4, sample 0Mo2.4Ni@900 had higher N and Ni contents than sample 0.27Mo2.4Ni@900; however, the former material exhibited lower HER activity (Figure 4 a,b). Thus, it can be inferred that the greatly high HER activity of the Mo_xC-Ni@NCV materials mainly depended on the molybdenum carbide (γ-MoC or β-Mo_2C) modification. However, with only β-Mo_2C modification, sample 0.27Mo0Ni@900 revealed much poorer HER activity than sample 0.27Mo2.4Ni@900.

It has been reported that γ-MoC is highly efficient to promote the overall electrocatalytic activity of noble metal catalysts due to its unique d-band electronic structures.[45] Herein, the introduction of γ-MoC into sample 0.27Mo2.4Ni@900 may play the crucial role in enhancing the HER activity of the Mo_xC-Ni@NCV catalysts. Further analysis indicated that the crystal Ni, γ-MoC contents, and graphitization degree were all reduced with the decrease of calcination temperature in the range 700–1000 °C (Figure S11). However, the overpotential (68–78 mV) at 10 mA cm^{-2} remained almost the same for these samples (Figure 4 c), which suggested that the contents of crystal Ni and γ-MoC as well as graphitization degree affected the HER activity faintly. While the calcination temperature reduced to 500 °C, there was not any γ-MoC formed in the products (Figure S11). Correspondingly, the obtained material (0.27Mo2.4Ni@500) showed an overpotential of 206 mV at 10 mA cm^{-2}, indicating an obviously lower HER activity than those of these samples modified with γ-MoC (Figure 4c). In addition, the introduction of Ni salts played an important role in affecting the metal phase and the catalytic performance. As shown in Figure S12, both γ-MoC and β-Mo_2C were formed with the introduction of Ni salts, which were in line with the above discussion. The performance of Mo_xC-Ni@NCV improved gradually with an increase in the Ni salts dosage, which suggested that the contents of crystal Ni affected the HER activity with the presence of γ-MoC. More importantly, when the Ni source ($NiCl_2 \cdot 6H_2O$) increased from 2.4 to 3.0 g, there was almost no Mo_2C phase in the products of sample 0.27Mo3.0Ni@900 (Figure 5). Correspondingly, the

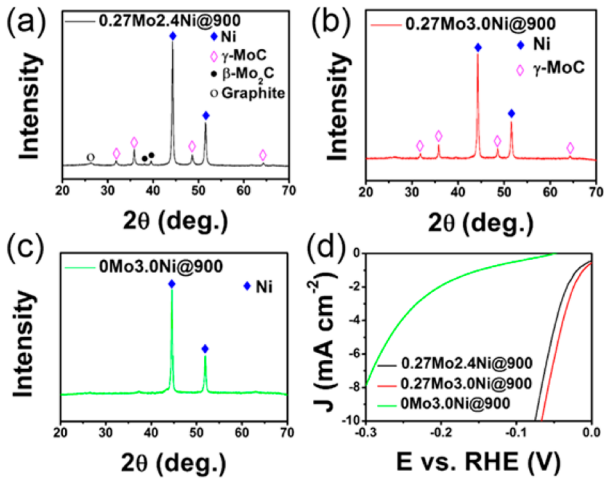

Figure 5. (a) XRD patterns of sample 0.27Mo2.4Ni@900 with a Ni source amount of 2.4 g. (b) The XRD patterns of sample 0.27Mo3.0Ni@900 and with a Ni source amount of 3.0 g. (c) The XRD patterns of sample 0Mo3.0Ni@900. (d) The polarization curves measured in 0.5 M H_2SO_4 for different samples.

obtained materials were still highly active for HER (Figure 5). Therefore, the γ-MoC modification was the key factor in the very high HER activity, which corresponded to the EIS measurements (Figure 4d). Generally, the semicircle in the low-frequency range of the Nyquist plots is related to the charge-transfer resistance R_{CT}, while the solution resistance R_S is implicit in the high-frequency range.[54] As shown in Figure 4d, sample 0.27Mo2.4Ni@900 revealed a R_{CT} of ~46 Ω, much smaller than the R_{CT} (~516 Ω) of sample 0Mo2.4Ni@900, which indicated a significantly faster reaction rate for HER. The

DOI: 10.1021/jacs.5b07924
J. Am. Chem. Soc. 2015, 137, 15753–15759

superior charge transfer and HER activity may result from the electronically synergistic effect of γ-MoC with the doped N and encapsulated Ni.

As an important catalytic performance aspect for HER, the durability of the prepared Mo_xC-Ni@NCV catalysts was further evaluated in acidic electrolyte. Representatively, the durability of sample 0.27Mo2.4Ni@800 was tested because of its highest HER activity. As shown in Figure 4e, the polarization curves were measured before the first CV and after 1000 CV sweeps between −142 and 108 mV in 0.5 M H_2SO_4. As observed, the HER overpotential of sample 0.27Mo2.4Ni@800 after 1000 CV sweeps during 50 000 s was almost the same as the initial overpotential. In addition, the long-term stability of the Mo_xC-Ni@NCV materials was also measured by extended electrolysis at fixed potentials, and the catalytic current almost remained 10 mA cm^{-2} at −68 mV (vs RHE) in 0.5 M H_2SO_4, which revealed better stability than the commercial Pt/C (the inset of Figure 4 e). It is worth mentioning that the hydrogen bubbles formed on the Mo_xC-Ni@NCV materials were smaller and more stable than those from Pt/C (see the video in the Supporting Information), which may cause negligible noise. More importantly, the stability achieved in a very broad potential window from −600 mV to 0 mV (vs RHE) was also studied (Figure S13), and it turned out that the overpotential of sample 0.27Mo2.4Ni@800 decreased only 17 mV after 3000 CV sweeps between −600 and 0 mV (vs RHE), which indicated that the prepared Mo_xC-Ni@NCV materials were favorable for a wide potential range. Thus, the prepared Mo_xC-Ni@NCV materials had not only very high HER activity but also excellent durability in acidic electrolyte.

Additional analysis was conducted to evaluate the catalytic performance of the prepared Mo_xC-Ni@NCV materials for HER in basic electrolyte. As shown in Figure 4 f, the overpotential for HER at 10 mA cm^{-2} was 126 mV over sample 0.27Mo2.4Ni@800. Although being far higher than the HER overpotential (23 mV) of Pt/C, this overpotential was less than the values exhibited by the majority of nonprecious metal catalysts for HER in basic electrolyte, confirming that the prepared Mo_xC-Ni@NCV materials were by far one of the most efficient NPMCs for HER in basic electrolyte (Table S6). In addition, sample 0.27Mo2.4Ni@800 revealed a Tafel slope of 93 mV/decade that was approximate to the Tafel slope (74 mV/decade) of Pt/C (Figure S14a). Nevertheless, the durability of sample 0.27Mo2.4Ni@800 was slightly better than that of Pt/C (Figure S14b).

CONCLUSIONS

In summary, we have reported the synthesis of molybdenum-carbide-modified N-doped carbon vesicle encapsulating Ni nanoparticles (Mo_xC-Ni@NCV) that had a hierarchically mesoporous structure and was proven to be a highly efficient nonprecious metal catalyst for hydrogen evolution reaction (HER). These Mo_xC-Ni@NCV materials were synthesized by a simple and economic solid-state thermolysis method, which employed the melamine-related composites of oxalate and molybdate with uniform Ni ion doping (Ni@MOM-com) as precursor. Significantly, due to the promotion of Ni ions in the Ni@MOM-com precursor, γ-MoC nanoparticles were effectively decorated on the N-doped carbon encapsulating Ni nanoparticles under a mild condition. As a result, the catalytic performance for HER was improved greatly, and a quiet low overpotential of 68 mV at 10 mA cm^{-2} was exhibited stably by the Mo_xC-Ni@NCV material in acidic electrolyte. This confirmed that the Mo_xC-Ni@NCV material was the best active nonprecious metal catalyst for HER in acidic electrolyte to date. Therefore, this work has made a significant breakthrough in the development of highly efficient, inexpensive HER catalysts that are promising for practical applications and commercialization.

ASSOCIATED CONTENT

Supporting Information

The Supporting Information is available free of charge on the ACS Publications website at DOI: 10.1021/jacs.5b07924.

Experimental details and characterization (PDF)
Pt/C (AVI)
Mo_xC-Ni@NCV (AVI)

AUTHOR INFORMATION

Corresponding Author

*chemwy@zju.edu.cn

Author Contributions

S.W. and J.W. contributed equally.

Notes

The authors declare no competing financial interest.

ACKNOWLEDGMENTS

This work was supported by the National Natural Science Foundation of China (21376208 & 91534114), the Zhejiang Provincial Natural Science Foundation for Distinguished Young Scholars of China (LR13B030001), the Specialized Research Fund for the Doctoral Program of Higher Education (J20130060), the Fundamental Research Funds for the Central Universities, the Program for Zhejiang Leading Team of S&T Innovation, the Partner Group Program of the Zhejiang University, and the Max-Planck Society are greatly appreciated.

REFERENCES

(1) Turner, J. A. *Science* **1999**, *285*, 687.
(2) Dresselhaus, M. S.; Thomas, I. L. *Nature* **2001**, *414*, 332.
(3) Turner, J. A. *Science* **2004**, *305*, 972.
(4) Schuldiner, S. *J. Electrochem. Soc.* **1959**, *106*, 891.
(5) Neyerlin, K. C.; Gu, W. B.; Jorne, J.; Gasteiger, H. A. *J. Electrochem. Soc.* **2007**, *154*, B631.
(6) Sheng, W. C.; Gasteiger, H. A.; Shao-Horn, Y. *J. Electrochem. Soc.* **2010**, *157*, B1529.
(7) McCrory, C. C.; Jung, S.; Ferrer, I. M.; Chatman, S. M.; Peters, J. C.; Jaramillo, T. F. *J. Am. Chem. Soc.* **2015**, *137*, 4347.
(8) Subbaraman, R.; Tripkovic, D.; Chang, K. C.; Strmcnik, D.; Paulikas, A. P.; Hirunsit, P.; Chan, M.; Greeley, J.; Stamenkovic, V.; Markovic, N. M. *Nat. Mater.* **2012**, *11*, 550.
(9) Jin, H. Y.; Wang, J.; Su, D. F.; Wei, Z. Z.; Pang, Z. F.; Wang, Y. *J. Am. Chem. Soc.* **2015**, *137*, 2688.
(10) Andreiadis, E. S.; Jacques, P. A.; Tran, P. D.; Leyris, A.; Chavarot-Kerlidou, M.; Jousselme, B.; Matheron, M.; Pecaut, J.; Palacin, S.; Fontecave, M.; Artero, V. *Nat. Chem.* **2013**, *5*, 48.
(11) He, C. Y.; Wu, X. L.; He, Z. Q. *J. Phys. Chem. C* **2014**, *118*, 4578.
(12) Ahn, S. H.; Hwang, S. J.; Yoo, S. J.; Choi, I.; Kim, H. J.; Jang, J. H.; Nam, S. W.; Lim, T. H.; Lim, T.; Kim, S. K.; Kim, J. J. *J. Mater. Chem.* **2012**, *22*, 15153.
(13) Cai, J.; Xu, L.; Wang, J. M.; Zhang, L. Y.; Zhou, H.; Zhong, Y.; Chen, D.; Fan, H. Q.; Shao, H. B.; Zhang, J. Q.; Cao, C. N. *Int. J. Hydrogen Energy* **2013**, *38*, 934.
(14) McKone, J. R.; Sadtler, B. F.; Werlang, C. A.; Lewis, N. S.; Gray, H. B. *ACS Catal.* **2013**, *3*, 166.
(15) Fosdick, S. E.; Berglund, S. P.; Mullins, C. B.; Crooks, R. M. *ACS Catal.* **2014**, *4*, 1332.

DOI: 10.1021/jacs.5b07924
J. Am. Chem. Soc. 2015, 137, 15753−15759

(16) Herraiz-Cardona, I.; Gonzalez-Buch, C.; Valero-Vidal, C.; Ortega, E.; Perez-Herranz, V. *J. Power Sources* **2013**, *240*, 698.
(17) Cobo, S.; Heidkamp, J.; Jacques, P. A.; Fize, J.; Fourmond, V.; Guetaz, L.; Jousselme, B.; Ivanova, V.; Dau, H.; Palacin, S.; Fontecave, M.; Artero, V. *Nat. Mater.* **2012**, *11*, 802.
(18) Morales-Guio, C. G.; Hu, X. L. *Acc. Chem. Res.* **2014**, *47*, 2671.
(19) Tran, P. D.; Nguyen, M.; Pramana, S. S.; Bhattacharjee, A.; Chiam, S. Y.; Fize, J.; Field, M. J.; Artero, V.; Wong, L. H.; Loo, J.; Barber, J. *Energy Environ. Sci.* **2012**, *5*, 8912.
(20) Kong, D. S.; Cha, J. J.; Wang, H. T.; Lee, H. R.; Cui, Y. *Energy Environ. Sci.* **2013**, *6*, 3553.
(21) Lukowski, M. A.; Daniel, A. S.; Meng, F.; Forticaux, A.; Li, L. S.; Jin, S. *J. Am. Chem. Soc.* **2013**, *135*, 10274.
(22) Tran, P. D.; Chiam, S. Y.; Boix, P. P.; Ren, Y.; Pramana, S. S.; Fize, J.; Artero, V.; Barber, J. *Energy Environ. Sci.* **2013**, *6*, 2452.
(23) Chen, W. F.; Sasaki, K.; Ma, C.; Frenkel, A. I.; Marinkovic, N.; Muckerman, J. T.; Zhu, Y. M.; Adzic, R. R. *Angew. Chem., Int. Ed.* **2012**, *51*, 6131.
(24) Cao, B. F.; Veith, G. M.; Neuefeind, J. C.; Adzic, R. R.; Khalifah, P. G. *J. Am. Chem. Soc.* **2013**, *135*, 19186.
(25) Chen, W. F.; Muckerman, J. T.; Fujita, E. *Chem. Commun.* **2013**, *49*, 8896.
(26) Vrubel, H.; Hu, X. L. *Angew. Chem., Int. Ed.* **2012**, *51*, 12703.
(27) McEnaney, J. M.; Crompton, J. C.; Callejas, J. F.; Popczun, E. J.; Biacchi, A. J.; Lewis, N. S.; Schaak, R. E. *Chem. Mater.* **2014**, *26*, 4826.
(28) Popczun, E. J.; McKone, J. R.; Read, C. G.; Biacchi, A. J.; Wiltrout, A. M.; Lewis, N. S.; Schaak, R. E. *J. Am. Chem. Soc.* **2013**, *135*, 9267.
(29) Xing, Z. C.; Liu, Q.; Asiri, A. M.; Sun, X. P. *Adv. Mater.* **2014**, *26*, 5702.
(30) Jahan, M.; Liu, Z. L.; Loh, K. P. *Adv. Funct. Mater.* **2013**, *23*, 5363.
(31) McArthur, M. A.; Jorge, L.; Coulombe, S.; Omanovic, S. *J. Power Sources* **2014**, *266*, 365.
(32) Wu, Z. X.; Lv, Y. Y.; Xia, Y. Y.; Webley, P. A.; Zhao, D. Y. *J. Am. Chem. Soc.* **2012**, *134*, 2236.
(33) Li, Y. G.; Wang, H. L.; Xie, L. M.; Liang, Y. Y.; Hong, G. S.; Dai, H. J. *J. Am. Chem. Soc.* **2011**, *133*, 7296.
(34) Tavakkoli, M.; Kallio, T.; Reynaud, O.; Nasibulin, A. G.; Johans, C.; Sainio, J.; Jiang, H.; Kauppinen, E. I.; Laasonen, K. *Angew. Chem., Int. Ed.* **2015**, *54*, 4535.
(35) Deng, D. H.; Yu, L.; Chen, X. Q.; Wang, G. X.; Jin, L.; Pan, X. L.; Deng, J.; Sun, G. Q.; Bao, X. H. *Angew. Chem., Int. Ed.* **2013**, *52*, 371.
(36) Deng, J.; Ren, P.; Deng, D.; Bao, X. *Angew. Chem., Int. Ed.* **2015**, *54*, 2100.
(37) Deng, J.; Ren, P. J.; Deng, D. H.; Yu, L.; Yang, F.; Bao, X. H. *Energy Environ. Sci.* **2014**, *7*, 1919.
(38) Zou, X. X.; Huang, X. X.; Goswami, A.; Silva, R.; Sathe, B. R.; Mikmekova, E.; Asefa, T. *Angew. Chem., Int. Ed.* **2014**, *53*, 4372.
(39) Esposito, D. V.; Hunt, S. T.; Stottlemyer, A. L.; Dobson, K. D.; McCandless, B. E.; Birkmire, R. W.; Chen, J. G. G. *Angew. Chem., Int. Ed.* **2010**, *49*, 9859.
(40) Esposito, D. V.; Chen, J. G. G. *Energy Environ. Sci.* **2011**, *4*, 3900.
(41) Esposito, D. V.; Hunt, S. T.; Kimmel, Y. C.; Chen, J. G. G. *J. Am. Chem. Soc.* **2012**, *134*, 3025.
(42) Chen, W. F.; Wang, C. H.; Sasaki, K.; Marinkovic, N.; Xu, W.; Muckerman, J. T.; Zhu, Y.; Adzic, R. R. *Energy Environ. Sci.* **2013**, *6*, 943.
(43) Wan, C.; Regmi, Y. N.; Leonard, B. M. *Angew. Chem., Int. Ed.* **2014**, *53*, 6407.
(44) Kelly, T. G.; Lee, K. X.; Chen, J. G. G. *J. Power Sources* **2014**, *271*, 76.
(45) Yan, Z. X.; He, G. Q.; Shen, P. K.; Luo, Z. B.; Xie, J. M.; Chen, M. *J. Mater. Chem. A* **2014**, *2*, 4014.
(46) Liao, L.; Wang, S. N.; Xiao, J. J.; Bian, X. J.; Zhang, Y. H.; Scanlon, M. D.; Hu, X. L.; Tang, Y.; Liu, B. H.; Girault, H. H. *Energy Environ. Sci.* **2014**, *7*, 387.
(47) Liu, Y.; Yu, G.; Li, G.-D.; Sun, Y.; Asefa, T.; Chen, W.; Zou, X. *Angew. Chem., Int. Ed.* **2015**, *54*, 10752.
(48) Zachariah, A.; Baiju, K. V.; Shukla, S.; Deepa, K. S.; James, J.; Warrier, K. G. K. *J. Phys. Chem. C* **2008**, *112*, 11345.
(49) Oshikawa, K.; Nagai, M.; Omi, S. *J. Phys. Chem. B* **2001**, *105*, 9124.
(50) Xiang, M. L.; Li, D. B.; Li, W. H.; Zhong, B.; Sun, Y. H. *Catal. Commun.* **2007**, *8*, 513.
(51) Zhi, L. J.; Hu, Y. S.; El Hamaoui, B.; Wang, X.; Lieberwirth, I.; Kolb, U.; Maier, J.; Müllen, K. *Adv. Mater.* **2008**, *20*, 1727.
(52) Chen, L. Y.; Bai, J. F.; Wang, C. Z.; Pan, Y.; Scheer, M.; You, X. Z. *Chem. Commun.* **2008**, 1581.
(53) El Hamaoui, B.; Zhi, L. J.; Wu, J. S.; Kolb, U.; Müllen, K. *Adv. Mater.* **2005**, *17*, 2957.
(54) Xie, J. F.; Zhang, H.; Li, S.; Wang, R. X.; Sun, X.; Zhou, M.; Zhou, J. F.; Lou, X. W.; Xie, Y. *Adv. Mater.* **2013**, *25*, 5807.

DOI: 10.1021/jacs.5b07924
J. Am. Chem. Soc. 2015, 137, 15753−15759